Myosin VI regulates gene pairing and transcriptional pause release in T cells

Cornelia E. Zorca[a,b,1], Lark Kyun Kim[a,c,1], Yoon Jung Kim[b,2], Matthew R. Krause[d], Daniel Zenklusen[e], Charalampos G. Spilianakis[a,3], and Richard A. Flavell[a,c,4]

Departments of [a]Immunobiology and [b]Genetics, and [c]Howard Hughes Medical Institute, Yale University School of Medicine, New Haven, CT 06520; [d]Montreal Neurological Institute, McGill University, Montreal, QC H3A 2B4, Canada; and [e]Département de Biochimie, Université de Montréal, Montreal, QC H3T 1J4, Canada

Contributed by Richard A. Flavell, February 12, 2015 (sent for review January 21, 2015; reviewed by Kenneth M. Murphy and Cornelis Murre)

Naive CD4 T cells differentiate into several effector lineages, which generate a stronger and more rapid response to previously encountered immunological challenges. Although effector function is a key feature of adaptive immunity, the molecular basis of this process is poorly understood. Here, we investigated the spatiotemporal regulation of cytokine gene expression in resting and restimulated effector T helper 1 (Th1) cells. We found that the *Lymphotoxin* (*LT*)/*TNF* alleles, which encode TNF-α, were closely juxtaposed shortly after T-cell receptor (TCR) engagement, when transcription factors are limiting. Allelic pairing required a nuclear myosin, myosin VI, which is rapidly recruited to the *LT/TNF* locus upon restimulation. Furthermore, transcription was paused at the *TNF* locus and other related genes in resting Th1 cells and released in a myosin VI-dependent manner following activation. We propose that homologous pairing and myosin VI-mediated transcriptional pause release account for the rapid and efficient expression of genes induced by an external stimulus.

homolog pairing | myosin VI | polymerase pausing | GRO-seq

Naive $CD4^+$ T cells have the potential to differentiate into several effector lineages (1), which play distinct roles in adaptive immune responses (2, 3). The polarization process is driven by many well-characterized transcription factors and epigenetic modifications. For instance, following T-cell receptor (TCR) and cytokine-mediated activation, naive $CD4^+$ T cells transcribe low levels of the alternatively expressed genes *IFN-γ* and *IL-4*, *IL-5*, and *IL-13*, irrespective of their ultimate effector lineage fate (4). During differentiation, however, contrasting activation patterns are established: T helper 1 (Th1) cells exclusively express the signature cytokine interferon-gamma (IFN-γ) in a T-bet–dependent manner, whereas Th2 cells exclusively express IL-4, IL-5, and IL-13 in a Gata3-dependent manner. These changes in transcriptional activity have been demonstrated by the appearance of DNase I hypersensitive sites, as well as by changes in histone acetylation and DNA methylation patterns (5–8). Furthermore, recent work has demonstrated that interchromosomal associations between cytokine genes play an important role in the differentiation process (9, 10). Overall, a vast array of transcription factors, epigenetic modifications, and long-range interactions are needed to establish the identity of effector Th cells. An important aspect of effector T-cell function is the rapid and efficient induction of cytokine gene expression upon antigen encounter. However, the precise spatial and temporal aspects of effector T-cell transcriptional activation are still largely unknown.

A fundamental feature of genome regulation is the spatial organization of genes into chromosomal territories. Although chromosomes occupy distinct territories in the nucleus, their location is cell type-specific and may change upon cellular activation. Notably, cell activation has been shown to promote extensive intermingling among chromosomal territories (11, 12). In addition, the position of individual genes can change with induction (13–15). For example, two coordinately regulated genes separated by 20 megabases (Mb) of linear genomic DNA, *HBB1* and *ERAF*, have been shown to associate at high frequency at shared sites of RNA polymerase II (RNAPII) transcription during erythroid differentiation (13). The spatial juxtaposition of these genes correlated well with their transcriptional potential. Notably, both actively transcribed and poised alleles of *HBB1* and *ERAF* were shown to localize to RNAPII transcription foci (13). From these findings, the spatial organization of the nucleus has emerged as a critical aspect of genome regulation. To date, few factors are known to regulate the nuclear localization of genes and their transcription status, but actin was demonstrated to be an important component of both processes (14, 16, 17).

With regard to the temporal aspects of gene regulation, it was traditionally thought that the formation of the preinitiation complex (PIC) was the rate-limiting step in transcription (18, 19). However, many recent studies have shown that regulation also occurs after the recruitment of the PIC to the promoter, and that regulatory processes control the transition of RNAPII from a paused state to an actively elongating state (20–23). Some of the factors involved in these processes have been identified, including the 5,6-Dichloro-1-beta-D-ribofuranosylbenzimidazole (DRB) sensitivity-inducing factor (DSIF), the negative elongation factor (NELF), and the positive transcription elongation factor (P-TEFb)

Significance

Our study examines an important aspect of adaptive immunity, namely, the process of effector T-cell activation, which leads to the enhanced expression of lineage-specific cytokine genes upon T-cell receptor (TCR) re-engagement. We found that the *TNF* locus undergoes TCR-induced homologous allelic pairing, which correlates with biallelic expression and requires a molecular motor, myosin VI. Furthermore, we identified a role for myosin VI in mediating the transition of RNA polymerase II (RNAPII) from pausing to productive elongation at cytokine and other related loci. We propose that homologous pairing and RNAPII pause release ensure a rapid and synchronous transcriptional response in effector T cells following antigen re-exposure.

Author contributions: C.E.Z., L.K.K., and R.A.F. designed research; C.E.Z., L.K.K., and Y.J.K. performed research; C.E.Z., L.K.K., Y.J.K., M.R.K., D.Z., C.G.S., and R.A.F. analyzed data; C.E.Z., L.K.K., and R.A.F. wrote the paper; D.Z. provided assistance with single-molecule FISH; and C.G.S. provided assistance with DNA FISH and critical advice.

Reviewers: K.M.M., Washington University; C.M., University of California, San Diego.

The authors declare no conflict of interest.

Data deposition: The global run-on sequencing data reported in this paper have been deposited in the ArrayExpress archive (accession no. E-MTAB-2381).

[1]C.E.Z. and L.K.K. contributed equally to this work.

[2]Present address: Department of Biological Sciences, The University of Texas at Dallas, Richardson, TX 75080.

[3]Present addresses: Institute of Molecular Biology and Biotechnology, Foundation for Research and Technology-Hellas, 70013 Heraklion, Crete, Greece; and Department of Biology, University of Crete, 70013 Heraklion, Crete, Greece.

[4]To whom correspondence should be addressed. Email: richard.flavell@yale.edu.

This article contains supporting information online at www.pnas.org/lookup/suppl/doi:10.1073/pnas.1502461112/-/DCSupplemental.

(18). The DSIF–NELF complex keeps RNAPII stalled at the promoter, whereas P-TEFb releases and phosphorylates the polymerase C-terminal domain, allowing productive elongation (24). Although RNAPII pausing is now widely recognized as a crucial step in transcription, the molecular details remain elusive.

In the present study, we took advantage of the fact that naive CD4$^+$ T cells can differentiate in vitro into effector Th1 cells (25), which then rapidly express TNF-α and IFN-γ upon TCR restimulation. We first investigated the role of nuclear positioning in the transcriptional regulation of these two cytokine genes in resting and restimulated Th1 cells using DNA FISH. Interestingly, we observed that unlike *IFN-γ*, the *TNF* alleles undergo homologous pairing. This event correlated with biallelic TNF-α transcription early upon TCR restimulation. Allelic pairing and RNAPII binding to the *TNF* promoter were significantly diminished both in the absence of myosin VI and upon deletion of the 5′ UTR of the *TNF* locus on both alleles. Using global run-on sequencing (GRO-seq), we found that transcription of TNF-α was paused at the promoter in resting Th1 cells but that upon restimulation, RNAPII pausing was released in a myosin VI-dependent manner. Finally, we identified several other genes, including *TBET* and *TNFAIP8*, which also showed myosin VI-dependent release of RNAPII pausing and homologous pairing. Taken together, our data suggest that RNAPII pausing and allelic pairing are general features of several inducible genes, facilitating a rapid and coordinated transcriptional response.

Results

***Lymphotoxin/TNF* Alleles Undergo Homologous Pairing in Th1 Cells Following TCR Restimulation.** Searching for factors that establish cell type-specific gene expression programs, we used 3D-DNA FISH to map the positions of the *Lymphotoxin* (*LT*)/*TNF* and *IFN-γ* loci over a time course of T-cell activation. TNF-α and IFN-γ mRNA expression were low in the naive CD4$^+$ precursors and remained low during differentiation into Th1 cells, but both cytokines were rapidly induced in Th1 cells upon TCR reengagement (Fig. 1*A* and Fig. S1*A*). Interestingly, the *LT*/*TNF* alleles, which were typically well-separated in resting Th1 cells, underwent substantial allelic pairing after 1 h of TCR stimulation. At later time points, the frequency of pairing decreased (Fig. 1 *B* and *C*). By contrast, the *IFN-γ* alleles did not undergo homologous pairing in the same cells in response to transcription activation (Fig. S1*B*). We defined paired alleles as loci separated by a distance of 1.5 μm or less based on Fisher's exact test performed in sliding windows (Fig. S1*C*).

To explore the functional significance of *LT*/*TNF* pairing, we asked whether this process correlates with transcription. Inhibition of transcription elongation with the reversible inhibitor DRB abrogated allelic pairing (Fig. S2 *A* and *B*), and removal of DRB after pretreatment restored it (Fig. S2*C*). We then assessed the allelic transcription status directly by RNA-DNA FISH (Fig. 1*D*). In the absence of TCR stimulation, the *LT*/*TNF* alleles were separate and transcriptionally silent in 72% of cells. Basal TNF-α expression, present in 14% of the cells, was primarily monoallelic and occurred from separate alleles (Fig. 1 *E* and *F*). By 1 h of stimulation, the frequency of both monoallelically and biallelically expressing cells had increased. Monoallelic TNF-α expression occurred from separate alleles (in 26% of cells), whereas biallelic expression occurred primarily from paired alleles (in 21% of cells). In addition, 36% of the cells with separate alleles and 14% of the cells with paired alleles were not transcribed at 1 h of stimulation. At 3 h after T-cell stimulation, the frequency of monoallelic expression remained the same, whereas the frequency of biallelic expression increased further. Both monoallelic (25%) and biallelic (48%) expression occurred primarily from separate alleles at this time point (Fig. 1 *E* and *F*). We conclude that allelic pairing is transient and correlates with biallelic TNF-α transcription at the earliest time point of restimulation.

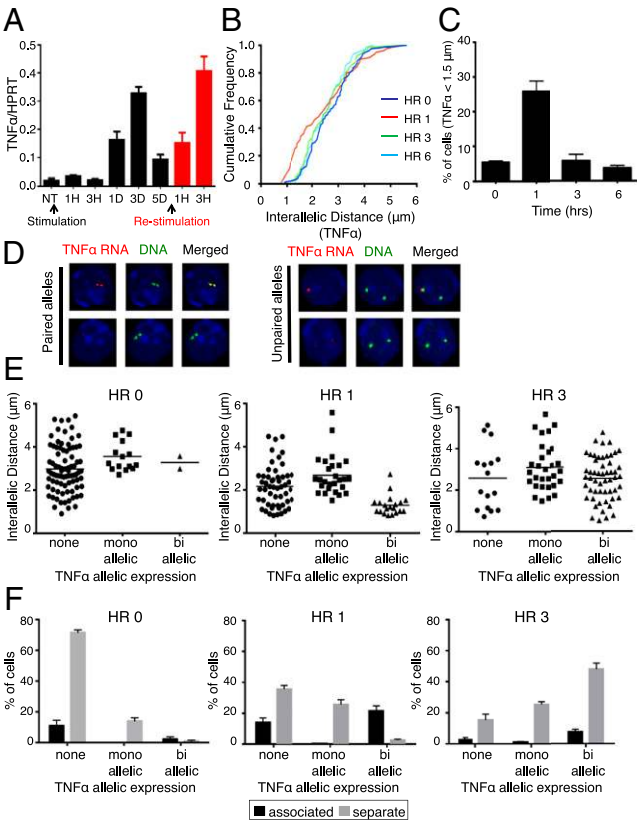

Fig. 1. Homologous pairing of the *LT*/*TNF* alleles correlates with biallelic TNF-α expression in 1-h restimulated Th1 cells. (*A*) Quantitative PCR of TNF-α mRNA expression in differentiating and restimulated Th1 cells. HPRT, hypoxanthine phosphoribosyltransferase. (*B*) Three-dimensional DNA FISH for the *LT*/*TNF* locus. The cumulative frequency plots display interallelic distances for the *LT*/*TNF* locus over a time course of 0–6 h of anti-CD3 treatment (n = 80 cells per time point, representative of three independent experiments). The Kolmogorov–Smirnov (KS) test was performed, and a P value <0.01 for hour (HR) 0 vs. HR 1 was obtained. (*C*) Percentage of Th1 effector cells showing an interallelic *LT*/*TNF* distance equal to or below 1.5 μm. The Student t test for HR 0 vs. HR 1 was performed ($P < 0.01$). (*D*) RNA-DNA FISH to map the position and the transcription status of the TNF-α alleles in single cells. The TNF-α RNA is shown in red, and the DNA locus is shown in green. Paired alleles exhibited an interallelic *LT*/*TNF* distance equal to or below 1.5 μm. (Magnification: 100×.) (*E*) Intranuclear separation of silent, monoallelically, and biallelically TNF-α–expressing cells (n = 100). (*F*) Percentage of silent, monoallelically, and biallelically TNF-α–expressing cells. Cells with an interallelic *LT*/*TNF* distance equal to or below 1.5 μm were scored as associated. Data are representative of at least three independent experiments.

Homologous Pairing of the *TNF* Alleles Depends on Nuclear Myosin VI. We next sought to understand the molecular basis of the transcription-associated *LT*/*TNF* pairing. Nuclear myosin VI, the only myosin that moves toward the minus end of actin filaments (26), has been previously shown to colocalize with RNAPII on the promoters of target genes and to enhance their transcription (27). Based on this finding, we reasoned that myosin VI might play a role in the homologous pairing of the *LT*/*TNF* alleles. We examined the position of this gene in resting and stimulated cells in the presence or absence of either the myosin VI inhibitor 2,4,6-triiodophenol (TIP) (28) or the actin inhibitor cytochalasin B. Both inhibitors effectively prevented TCR-induced pairing of the *LT*/*TNF* alleles (Fig. 2*A*). Inhibitors of other myosin family members had no effect (Fig. S3). Furthermore, we carried out DNA FISH combined with chromosome painting using chromosome 17 and *TNF* locus probes in myosin VI$^{+/-}$ and myosin VI$^{-/-}$ Th1 cells (29). T-cell development in myosin VI-deficient

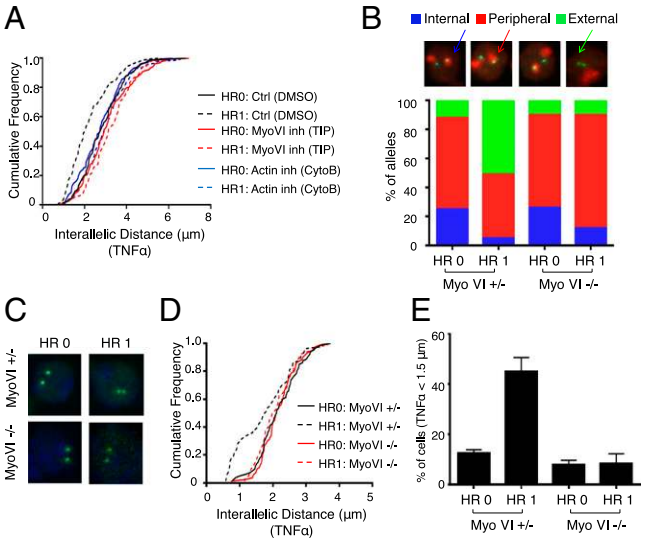

Fig. 2. Pairing and repositioning of the *LT/TNF* locus are dependent on nuclear myosin VI. (*A*) Separation of the homologous *LT/TNF* alleles was measured in resting or 1-h restimulated Th1 cells in the presence or absence of either TIP or cytochalasin B (CytoB) ($n = 100$). inh, inhibitor; Myo VI, myosin VI. The KS test was performed, and a *P* value <0.01 for HR 0 vs. HR 1 for the DMSO control was obtained. (*B*) Localization of the *LT/TNF* alleles relative to the chromosomal territory was determined by chromosome painting (red) combined with DNA FISH (green) in resting (HR 0) and 1-h restimulated (HR 1) Myo VI$^{+/-}$ and Myo VI$^{-/-}$ Th1 cells. Data are representative of three independent experiments. (*C*) Separation of the homologous *LT/TNF* alleles was measured in resting (HR 0) or 1-h restimulated (HR 1) Myo VI-sufficient or Myo VI-deficient Th1 cells by DNA FISH. The *LT/TNF* locus is shown in green. (*D*) Cumulative frequency plots of distances between the homologous *LT/TNF* alleles. The KS test was performed, and a *P* value <0.01 for HR 0 vs. HR 1 Myo VI$^{+/-}$ Th1 cells was obtained. (*E*) Percentage of resting and 1-h restimulated Myo VI$^{+/-}$ and Myo VI$^{-/-}$ Th1 cells showing an interallelic *LT/TNF* separation equal to or below 1.5 μm. Data represent three independent experiments. The Student *t* test for HR 0 vs. HR 1 Myo VI$^{+/-}$ cells was performed, and a *P* value <0.01 was obtained. (Magnification: *B*, 60×; *C*, 100×.)

mice showed no obvious defects and was comparable to T-cell development in myosin VI-sufficient mice (Fig. S4 *A* and *B*). In resting cells of either genotype, the *LT/TNF* alleles were located predominantly at the periphery (63%) or, to a lesser extent, in the interior (25%) of the chromosomal territory (Fig. 2*B*). Upon activation, however, the alleles assumed an external position in a much greater proportion of myosin VI-sufficient (51%) than myosin VI-deficient (10%) cells. Consistent with the effect of myosin VI inhibition by TIP, loss of myosin VI activity disrupted *LT/TNF* pairing (Fig. 2 *C–E*). The accumulation of mature TNF-α and IFN-γ mRNA seemed, however, to be similar in myosin VI-sufficient and myosin VI-deficient T cells during the several-day process of differentiation of naive T cells into effector Th1 cells (Fig. S4*C*). This result raises the possibility that the effect of myosin VI on mature cytokine mRNA accumulation may be redundant with the effect of other myosin family members. We hypothesized that if myosin VI plays a role in gene expression, it acts transiently and regulates an early step in transcription activation following restimulation.

Myosin VI Mediates the Transition of RNAPII from Pausing to Productive Elongation. Specifically, we asked whether myosin VI regulates transcription initiation, pausing, or elongation of cytokine genes in restimulated Th1 cells. Several studies have shown that RNAPII pausing is prevalent at genes involved in signaling pathways (18, 22, 30–33). We used GRO-seq to measure nascent transcription genome-wide in the presence or absence of nuclear myosin VI. Interestingly, TCR engagement induced a decrease in RNAPII pausing across the genome in myosin VI-sufficient cells but not in myosin VI-deficient cells, suggesting a global role for myosin VI in mediating RNAPII pause release (Fig. 3*A*). In addition, we performed metagene analyses of genes that were significantly activated by TCR re-engagement ($P < 1E\text{-}16$). Our data showed that the change in reads per kilobase of gene per million mapped sequence reads (RPKM) between $t = 0$ and $t = 1$ was clearly different for myosin VI-sufficient and myosin VI-deficient Th1 cells (Fig. 3*B*). Specifically, in myosin VI-sufficient cells, the promoter RPKM decreased and the gene body RPKM increased dramatically with stimulation compared with the resting state. By contrast, in myosin VI-deficient cells, both the promoter RPKM and the gene body RPKM increased only slightly with stimulation compared with the resting state. The accumulation of RPKM in the promoter proximal region in stimulated myosin VI-deficient cells suggests a transcription elongation defect.

Furthermore, the GRO-seq tag density in the promoter-proximal region of the *TNF* locus and the *TBX21* locus, encoding the transcription factor T-bet, was high in resting Th1 cells, whereas the tag density in the gene body was low. This observation suggests that these genes are paused. Transcription elongation proceeded rapidly after TCR activation in both myosin VI-sufficient and myosin VI-deficient cells; however, the tag density was lower along the *TNF* and *TBX21* gene body in myosin VI-deficient cells (Fig. 3*C*). Consistent with the results for the *TNF* locus, the *TBX21* alleles showed a similar activation-

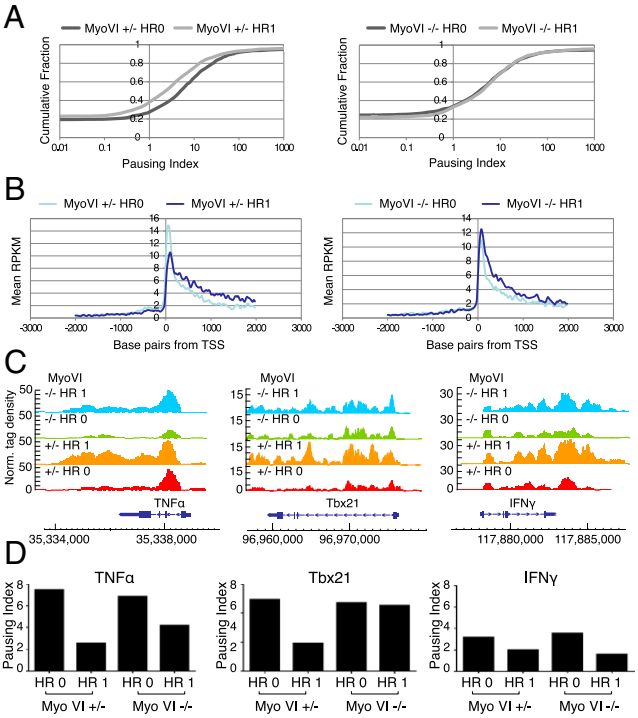

Fig. 3. Nuclear Myo VI regulates RNAPII pausing. (*A*) Cumulative fraction plot of PI values for all transcribed genes in resting (dark gray: HR 0) and restimulated (light gray: HR 1) Myo VI-sufficient (*Left*) and Myo VI-deficient (*Right*) Th1 cells. (*B*) Metagene profiles of resting (light blue: HR 0) and restimulated (dark blue: HR 1) myosin VI-sufficient (*Left*) and myosin VI-deficient (*Right*) Th1 cells. The *y* axis shows the mean RPKM of GRO-seq tag densities between 2,000 bp upstream and 2,000 bp downstream of the transcription start site (TSS). The *x* axis represents base pairs from the TSS. (*C*) GRO-seq profiles of the *TNF-α*, *TBX21*, and *IFN-γ* loci in resting and 1-h restimulated myosin VI$^{+/-}$ and myosin VI$^{-/-}$ Th1 cells. Norm., normalized. (*D*) PI of RNAPII for the *TNF-α*, *TBX21*, and *IFN-γ* loci.

dependent association (Fig. S5*A*). In contrast, at the *IFN-γ* locus (whose alleles did not associate), we did not find substantial differences in the tag density profiles (Fig. 3*C*). To assess the degree of RNAPII pausing and release, we calculated the pausing index (PI), defined as the read density within 300 bp of the transcription start site divided by the read density in the gene body (34, 35). A high PI value indicates pausing. In myosin VI-sufficient cells, the PI for the *TNF* and *TBX21* loci was reduced after TCR activation, indicating release of paused RNAPII (Fig. 3*D*). In myosin VI-deficient cells, however, this PI decrease was less pronounced than in myosin VI-sufficient cells. In contrast, at the *IFN-γ* locus, the PI decreased with TCR activation in both myosin VI-sufficient and myosin VI-deficient cells, indicating that RNAPII elongation in the *IFN-γ* gene is not regulated by myosin VI (Fig. 3*D*). We therefore infer that myosin VI affects the rate at which RNAPII transitions into productive elongation at target loci. Moreover, we used the GRO-seq data to look for other up-regulated genes with a resting PI similar to *TNF*. One of these genes, *TNFAIP8*, showed a myosin VI-dependent decrease in the PI and homologous pairing upon TCR activation, whereas the other two, *NCL* and *TAPT1*, were myosin VI-independent and did not show pairing (Fig. S5 *B–D*).

To confirm the GRO-seq results, we examined the expression of nascent TNF-α transcripts at different points along the gene by quantitative PCR (qPCR) analysis after the removal of mature poly(A)$^+$ RNA (Fig. S6). Interestingly, the level of TNF-α nascent RNA was similar in restimulated myosin VI-sufficient and myosin VI-deficient cells when quantified with the 5′ UTR/exon 1 primer set, but it was significantly lower in myosin VI-deficient compared with myosin VI-sufficient cells in all other downstream regions (Fig. S6*A*). This result corroborates the GRO-seq data and suggests that myosin VI-deficient cells have a transcription elongation defect. We observed a similar pattern for the *TBX21* gene (Fig. S6*B*); in this case, we found an elongation defect at the exon 2/intron 2 junction. Notably, the first intron of the *TBX21* gene is very long, whereas the first intron of the *TNF* gene is not (Fig. 3*C*). We think this distinct feature is one of the possible explanations for the difference in the site of pausing found at the *TNF* vs. *TBX21* locus. Further studies will be needed to explore this observation.

Myosin VI Is Recruited to Target Genes in Response to TCR Restimulation. To investigate the role of myosin VI further in the switch from transcriptional pausing to productive elongation, we examined the binding profiles of the two isoforms of RNAPII that have been associated with these states (36, 37). In resting myosin VI-sufficient cells, initiation RNAPII-Ser5P was predominantly bound to the *TNF* promoter. TCR engagement resulted in a decrease in this isoform and a concomitant increase in the elongation RNAPII-Ser2P levels (Fig. 4*A*). Notably, in TCR-stimulated myosin VI-deficient cells, the increase in RNAPII-Ser2P levels was significantly lower than in myosin VI-sufficient cells (Fig. 4*A*). In addition, examination of the 3′ end of the *TNF* gene revealed that higher levels of RNAPII-Ser2P were present in stimulated compared with resting myosin VI-sufficient cells. This increase was attenuated in myosin VI-deficient cells, supporting a role for myosin VI in transcription elongation. Finally, we examined the binding profile of Spt5, a factor known to induce promoter-proximal pausing (30, 38), in Th1 cells. High levels of Spt5 were bound to the *TNF* promoter in resting cells, which decreased significantly following TCR activation (Fig. 4*B*). Taken together, these results are consistent with the GRO-seq data and suggest that myosin VI regulates the transition of RNAPII from pausing to productive elongation.

To determine whether myosin VI regulates its target genes directly, we examined its binding profile over a time course of TCR activation by ChIP. In resting Th1 cells, low levels of myosin VI were bound to the *TNF* and *IFN-γ* loci (Fig. 4*C*). TCR activation,

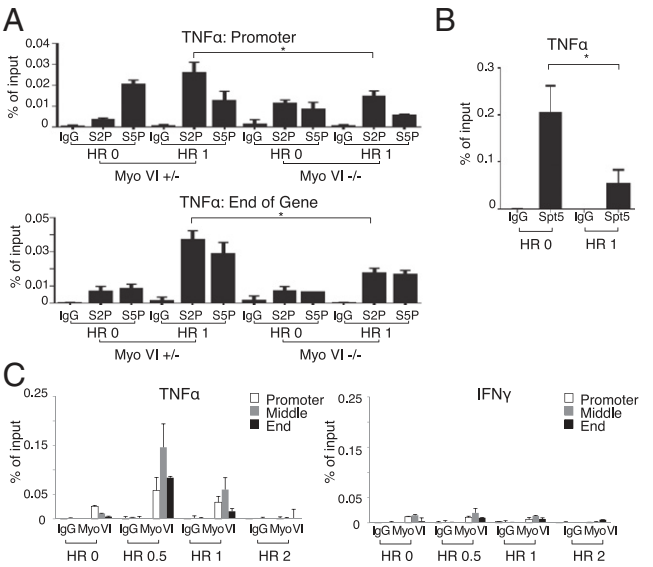

Fig. 4. Nuclear Myo VI regulates the switch between poised and elongating RNAPII following TCR restimulation. (*A*) ChIP-qPCR binding profiles of RNAPII-Ser2P and RNAPII-Ser5P on the *TNF* promoter and at the 3′ end of the gene in resting (HR 0) and 1-h restimulated (HR 1) Myo VI$^{+/-}$ and Myo VI$^{-/-}$ Th1 cells. Data are averages of three independent experiments. The Student *t* test was performed (*$P < 0.05$). (*B*) ChIP-qPCR binding profile of Spt5 on the *TNF* promoter in resting (HR 0) and 1-h restimulated (HR 1) WT Th1 cells. Data are averages of three independent experiments. The Student *t* test was performed (*$P < 0.05$). (*C*) ChIP-qPCR binding profiles of Myo VI along cytokine genes over a time course (0, 0.5, 1, and 2 h) of anti-CD3 restimulation in WT Th1 cells. The results are representative of three independent experiments.

however, led to the recruitment of myosin VI to the *TNF* locus, but not to the *IFN-γ* locus, within 30 min (*IFN-γ* showed neither allelic pairing nor myosin VI-dependent pausing). Moreover, using immuno-RNA FISH, we found that the active *TNF* alleles colocalized with punctate myosin VI foci in restimulated Th1 cells (Fig. S7). By 2 h, the levels of myosin VI bound to the *TNF* locus decreased. Thus, the transient binding of myosin VI to target loci correlates well with the reduction in *TNF* pairing observed at late time points of stimulation (Figs. 4*C* and 1*C*, respectively).

Disruption of Homologous Allelic Pairing Alters TNF-α Expression in Th1 Cells. Finally, we asked whether disruption of allelic pairing affects TNF-α mRNA expression. We examined T cells harboring a deletion spanning from the 5′ UTR through the first intron of the *TNF* locus (Fig. 5*A*). This small deletion was designed to leave the promoter intact and allow RNAPII binding. However, we cannot exclude the possibility that the deletion also affects the distance between the promoter and regulatory elements, which may have consequences on transcription. We found that *TNF*$^{+/+}$ and *TNF*$^{+}$/5′Δ cells exhibited similar TCR-induced *TNF* allelic pairing profiles. In contrast, *TNF* 5′Δ/5′Δ cells showed no homologous *TNF* pairing. The association of the *TBX21* alleles was not affected by deletion of the *TNF* locus on either one or both alleles (Fig. 5*B*). Interestingly, the TNF-α nascent RNA levels beyond the deleted region (at the exon 2/intron 2 junction) were reduced in *TNF* 5′Δ/5′Δ cells compared with *TNF*$^{+/+}$ cells (Fig. 5*C*). We also observed loss of homologous pairing and decreased TNF-α transcript levels in T cells harboring a larger deletion (Fig. S8 *A–D*). Additionally, in *TNF* 5′Δ/5′Δ Th1 cells in which the promoter was intact, we observed that significantly less RNAPII-Ser5P, RNAPII-Ser2P, and myosin VI were bound to the *TNF* promoter and gene body under both resting and restimulated conditions compared with *TNF*$^{+/+}$ cells (Fig. 5 *D* and *E*). The observed decrease in TNF-α nascent RNA levels in TNF 5′Δ/5′Δ cells was not the

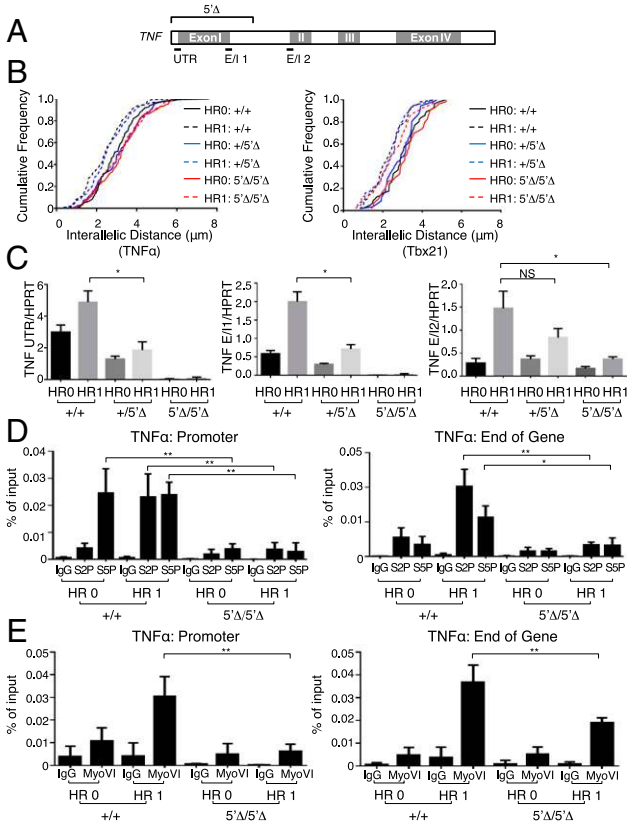

Fig. 5. Loss of homologous pairing disrupts TNF-α transcription. (*A*) Genomic organization of the *TNF* locus. The *TNF* 5′ deletion spans from the 5′ UTR through the first intron of the gene. (*B*) Cumulative frequency plots display the separation of the homologous *TNF* (*Left*) and *TBX21* (*Right*) alleles in resting (HR 0) or 1-h restimulated (HR 1) $TNF^{+/+}$, $TNF^{+}/5'\Delta$, and *TNF* 5′Δ/5′Δ Th1 cells ($n = 100$ cells, representative of three independent experiments). (*C*) qPCR analysis of nascent TNF-α mRNA expression in resting or 1-h restimulated $TNF^{+/+}$, $TNF^{+}/5'\Delta$, and *TNF* 5′Δ/5′Δ Th1 cells. The primers for qPCR were located within the 5′ UTR (*TNF* UTR), at the first exon/intron boundary (*TNF* E/I 1) or further along the gene body (*TNF* E/I 2). The results are averages of three independent experiments. The Student *t* test was performed (*$P < 0.05$; NS, not significant). ChIP-qPCR binding profiles of RNAPII-Ser5P (S5P) and RNAPII-Ser2P (S2P) (*D*) and Myo VI (*E*) on the *TNF* promoter and at the 3′ end of the gene in resting (HR 0) and 1-h restimulated (HR 1) $TNF^{+/+}$ and *TNF* 5′Δ/5′Δ Th1 cells. Data are averages of three independent experiments. The Student *t* test was performed (*$P < 0.05$; **$P < 0.01$).

result of reduced production of TNF-α, for example, acting exogenously on the cells, because TNF-α mRNA levels were comparable in *TNFR* WT and *TNFR* double-KO cells (which cannot respond to TNF-α) over the time course of differentiation and activation examined (Fig. S8*E*). Further, the addition of neutralizing TNF-α antibodies to the culture medium did not affect *TNF* allelic pairing (Fig. S8*F*). From these results, we conclude that homologous allelic pairing enhances *TNF* gene activation.

Discussion

Several reports have shown that the intranuclear position of a gene is linked to gene expression and that active loci colocalize to specific regions of the nucleus (13, 39). Our findings suggest that myosin VI participates in the reorganization of the genome in response to external stimuli. In particular, our observation that myosin VI-dependent homologous allelic pairing correlates with biallelic gene expression early upon TCR stimulation suggests that pairing modulates both the timing and the extent of gene expression. Furthermore, we found that myosin VI regulates transcription through release of RNAPII pausing. This finding is consistent with previous reports that have demonstrated a role for myosin I and actin in transcription and chromatin remodeling, respectively (40, 41).

We propose the following model for pairing-enhanced transcription. Early upon TCR activation, the *TNF* alleles associate by looping out of the chromosomal territory and colocalize at a shared nuclear body, which may be a favorable environment for transcription. Our finding that myosin VI has a punctate distribution in the nucleus may indeed indicate such a body. We speculate that these myosin VI foci contain additional factors (e.g., transcription factors, chromatin remodeling factors), which may be limiting in the initial phase of TCR signaling. Homologous alleles found in proximity to one another may share these factors more effectively. Furthermore, interallelic associations may increase the availability of the DNA target. As TCR signaling continues and more transcription factors become available, biallelic transcription can initiate on separate alleles or the previously associated alleles can drift apart while continuing to be transcribed. The possibility that the alleles pair, activate transcription, and then drift apart but continue to express TNF-α remains to be tested when live-cell imaging becomes available.

Additionally, we found that in the absence of myosin VI, the switch from poised to elongating RNAPII was defective. We present three lines of evidence: (*i*) by ChIP, we showed that less RNAPII-Ser2P was bound to the *TNF* promoter and gene body upon restimulation in myosin VI-deficient compared with myosin VI-sufficient cells (Fig. 4*A*); (*ii*) by nascent transcript qPCR, we showed that the nascent TNFα levels were significantly reduced in myosin VI-deficient compared with myosin VI-sufficient cells (Fig. S6*A*); and (*iii*) by GRO-seq, we found that myosin VI-deficient cells showed defects in the dynamics of *TNF* transcription elongation upon activation. The molecular mechanism whereby myosin VI regulates transcription during TCR activation remains to be elucidated, but we speculate that myosin VI acts either directly or indirectly to reduce the residence time of RNAPII at pause sites. To date, only a few molecules have been shown to enhance the elongation rate of RNAPII, including human Spt5 homologs and eleven–nineteen lysine-rich leukaemia (ELL) (42–44). Myosin VI may be part of a larger protein complex, working in conjunction with other factors to stimulate productive elongation.

Although we cannot directly link RNAPII pausing and gene paring, we successfully used the GRO-seq dataset to identify additional genes that exhibit myosin-dependent pausing and, by subsequent microscopic analysis, allelic pairing. For example, like *TNF*, the *TBX21* and *TNFAIP8* genes showed myosin VI-dependent RNAPII pause release by GRO-seq and myosin VI-dependent pairing by DNA FISH. In contrast, the expression of the *NCL*, *TAPT1*, and *IFN-γ* genes was myosin VI-independent, and these genes did not show homologous pairing. We currently do not know what features distinguish myosin VI-dependent genes from independent genes. Recent work has demonstrated that in human K652 cells, genes with short (250–500 bp) first exons have higher levels of H3K4me3 and H3K9ac in the promoter region and are more highly transcribed than genes with long first exons (45). Another possibility, besides gene structure and chromatin modifications, includes primary DNA sequence elements (23, 46). Future work will focus on elucidating these differences.

In summary, we found that nuclear myosin VI plays a dual role during the early time window of gene activation by participating in the reorganization of the genome and by modulating the transition of RNAPII from pausing to productive elongation. Both nuclear localization and RNAPII pausing may ensure a rapid and synchronous transcriptional response (18). Precisely how these two processes are interconnected remains to be elucidated until a live-cell imaging approach becomes available. Nevertheless, subnuclear localization and RNAPII pausing are emerging as critical regulatory events (18, 35, 47–49), which play a role in regulating a multitude of cellular responses.

Materials and Methods

Mice. C57BL/6 mice were obtained from the National Cancer Institute. *LT-β/TNF-α/LT-α* triple-KO mice (referred to as Δ3 KO mice), *TNF* 5′Δ KO mice, and myosin VI KO mice were obtained from the Jackson Laboratory and expanded into a colony at the Yale University Animal Resource Center. Animal care was in accordance with Yale's Institutional Animal Care and Use Committee regulations.

Reagents. The transcriptional inhibitor DRB and the myosin V inhibitor myovin-1 (475984) were purchased from Calbiochem. The myosin VI inhibitor TIP and the actin inhibitor cytochalasin B were purchased from Sigma. The myosin II inhibitor blebbistatin (BML-EI315-0005) was purchased from Enzo Life Sciences. All myosin inhibitors were used at a concentration equal to twice the IC_{50} (10 μM blebbistatin, 12 μM myovin-1, and 4 μM TIP) (50). The cells were pretreated with the inhibitors for 30 min and restimulated with αCD3 for 1 h. The TNF-α neutralizing antibody was purchased from Cell Signaling (11969). Chromosome 17-Texas Red paints (D-1417-050-TR) were purchased from MetaSystems.

T-Helper Cell Culture and Stimulation. $CD4^+$ T cells were isolated from the spleens, axillary, and inguinal lymph nodes of 6- to 8-wk-old C57BL/6 myosin $VI^{+/-}$ and myosin $VI^{-/-}$ mice or only from the spleens of Δ3 WT, heterozygous, and KO littermate mice. Total $CD4^+$ T-cell isolation was done by positive selection with MACS CD4 (L3T4) beads (Miltenyi Biotec, Inc.). Naive $CD62L^{high}CD44^{low}CD4^+Nk.1.1^-CD25^-$ T cells were purified by flow cytometric cell sorting (using flow-activated cell sorting). For in vitro differentiation toward the Th1 lineage, 1.5×10^6 naive CD4 T cells were stimulated with plate-bound αCD3 (10 mg/mL; clone 145-2C11, American Type Culture Collection) and αCD28 (2 mg/mL; Pharmingen) mouse antibodies in complete Click's medium (Irvine Scientific) in the presence of 50 U/mL rhIL-2 (Peprotech), 3.5 ng/mL murine rIL-12 (a generous gift from the Genetics Institute), and 10 mg/mL 11B11 (anti–IL-4). After 4–5 d of in vitro differentiation, the cells were harvested, separated in a Ficoll gradient, and stimulated with plate-bound αCD3 (10 mg/mL) over a time course.

Probe Synthesis for FISH. The templates for nick translation were the BACs RP24-352N22 (*IFN-γ*) and RP24-273L24 (*LT/TNF*) from the Children's Hospital Oakland Research Institute for DNA FISH and a 1-kb intron/exon spanning segment of the *TNF-α* gene cloned in pCR4 TOPO (Invitrogen) for RNA FISH. The DNA FISH probes were labeled by nick translation (32-801300; Vysis) with Spectrum Green dUTP or Spectrum Orange dUTP (Enzo Life Sciences) according to the manufacturer's instructions. The RNA FISH template was labeled by nick translation using a Biotin Nick Translation Kit (11745824910; Roche). Stellaris RNA FISH probes from Biosearch Technologies were used for immuno-RNA FISH.

FISH. For DNA FISH, the cells were harvested, resuspended in 1× PBS, attached onto poly-L-lysine–coated coverslips (354085; BD Bioscience), fixed with 4% (vol/vol) paraformaldehyde (pH 7.2) for 10 min, washed three times with 1× PBS, and permeabilized in 0.5% Triton X-100 in PBS for 10 min at room temperature. Following three washes with 1× PBS, the cells were incubated with 20% (vol/vol) glycerol in PBS for 30 min at room temperature before being flash-frozen in liquid nitrogen three times. Subsequently, the cells were washed with 1× PBS, and the DNA was depurinated with 0.1 N of HCl for 5 min. The cells were washed with 1× PBS and stored in 70% (vol/vol) ethanol. Before hybridization, the cells were dehydrated, air-dried, and denatured in 70% (vol/vol) formamide/2× SSC for 10 min at 75 °C. The cells were rinsed with ice-cold 1× PBS on ice and hybridized with the probe mix (preannealed with murine Cot-1 DNA) on slides overnight at 37 °C. Three posthybridization washes were carried out at room temperature in 2× SSC for 5 min each, and the samples were mounted with ProLong Gold antifade reagent with DAPI (P36935; Invitrogen). Images were acquired using a Leica TCS SP5 or a PerkinElmer Spinning Disk confocal microscope. For RNA-DNA FISH, the cells were permeabilized before fixation. The RNA FISH probe was detected using mouse antibiotin and goat anti-mouse IgG conjugated to Alexa Fluor 594. For immuno-RNA FISH, single-molecule RNA FISH was done as previously described (51), followed by immunostaining for myosin VI. Myosin VI antibodies were a kind gift from Mark Mooseker, Yale University, New Haven, CT.

Distance Measurements. Distances between DNA FISH signals were measured in three dimensions using Volocity (Improvision). Two to three independent cell preparations were analyzed, and 80–100 nuclei were scored per time point for each experiment.

Quantitative RT-PCR. RNA was isolated from sorted naive $CD4^+$ T cells and from resting and restimulated Th1 cells using TRIzol reagent (Invitrogen). cDNA was synthesized with oligo dT primers or with random hexamers using SuperScript II (Invitrogen) from three independent samples. For the nascent RNA qPCR analysis, mature poly(A)$^+$ RNA was removed using oligo (dT) 25-cellulose beads (New England Biolabs). The PCR assay was performed in duplicate on a 7500 ABI Real-Time PCR System (Applied Biosystems) using TaqMan probes (Applied Biosystems) or SYBR Green. The ΔC_T (delta threshold cycle) method was used for quantification, and cytokine transcripts were normalized to β-actin.

ChIP. ChIP was performed as described previously (52). Antibodies were purchased from Abcam for the RNAPII C-terminal domain (phospho S2, ab5095; phospho S5, ab5131), from Santa Cruz for Spt5 (sc-28678x), and from Sigma for myosin VI (M0691). The precipitated chromatin fragments were quantitated with the KAPA SYBR Fast qPCR kit (KK4600) in a 7500 ABI Real-Time PCR System (Applied Biosystems).

GRO-seq. GRO-seq and data analysis were performed as described previously (34). A total of 8–10 million T cells isolated and sorted from three to five myosin VI-sufficient or myosin VI-deficient mice were pooled per sample. The data shown represent one round of sequencing. The GRO-seq read depth was 10 million reads. The RPKM normalization method was used (53).

Accession Number. GRO-seq data are deposited in the ArrayExpress archive. The accession number is E-MTAB-2381.

Statistical Analysis. The Student *t* test was performed for all studies using GraphPad Prism 6.0. Allelic distance distributions were compared by the Kolmogorov–Smirnov test, and a *P* value was obtained using Prism 6.0 or Minitab 16 (Minitab). Homologous alleles separated by a distance of 1.5 μm or less were considered to be associated by Fisher's exact test performed using R. A P value <0.05 was considered statistically significant.

ACKNOWLEDGMENTS. We thank Dr. David Schatz, Dr. Tian Chi, Dr. Mark Mooseker, Dr. Adam Williams, Dr. Nicola Gagliani, Dr. Eran Elinav, Dr. Mariann Micsinai, and Dr. Paul Dieffenbach for helpful discussions. We are grateful to Dr. Julie Chaumeil, Dr. Jane Skok, and Samir Rahman for technical advice and to Caroline Lieber for assistance with preparation of the manuscript. We also thank Thomas R. Taylor and Gouzel Tokmoulina for cell sorting. C.E.Z. was the recipient of NIH Predoctoral Training Grant T32-GM07499. D.Z. was supported by the Canadian Institutes of Health Research (CIHR) (MOP-BMB-232642) and was the recipient of Fonds de recherche du Québec-Santé Chercheur Boursier Junior I. This work was supported by the Howard Hughes Medical Institute (L.K.K. and R.A.F.).

1. Zhu J, Yamane H, Paul WE (2010) Differentiation of effector CD4 T cell populations (*). *Annu Rev Immunol* 28:445–489.
2. Ahmed R, Gray D (1996) Immunological memory and protective immunity: Understanding their relation. *Science* 272(5258):54–60.
3. Zinkernagel RM, et al. (1996) On immunological memory. *Annu Rev Immunol* 14: 333–367.
4. Grogan JL, et al. (2001) Early transcription and silencing of cytokine genes underlie polarization of T helper cell subsets. *Immunity* 14(3):205–215.
5. Agarwal S, Avni O, Rao A (2000) Cell-type-restricted binding of the transcription factor NFAT to a distal IL-4 enhancer in vivo. *Immunity* 12(6):643–652.
6. Lee HJ, et al. (2000) GATA-3 induces T helper cell type 2 (Th2) cytokine expression and chromatin remodeling in committed Th1 cells. *J Exp Med* 192(1):105–115.
7. Fields PE, Lee GR, Kim ST, Bartsevich VV, Flavell RA (2004) Th2-specific chromatin remodeling and enhancer activity in the Th2 cytokine locus control region. *Immunity* 21(6):865–876.
8. Lee DU, Agarwal S, Rao A (2002) Th2 lineage commitment and efficient IL-4 production involves extended demethylation of the IL-4 gene. *Immunity* 16(5): 649–660.
9. Spilianakis CG, Lalioti MD, Town T, Lee GR, Flavell RA (2005) Interchromosomal associations between alternatively expressed loci. *Nature* 435(7042):637–645.
10. Kim LK, et al. (2014) Oct-1 regulates IL-17 expression by directing interchromosomal associations in conjunction with CTCF in T cells. *Mol Cell* 54(1):56–66.
11. Branco MR, Pombo A (2006) Intermingling of chromosome territories in interphase suggests role in translocations and transcription-dependent associations. *PLoS Biol* 4(5):e138.
12. Branco MR, Branco T, Ramirez F, Pombo A (2008) Changes in chromosome organization during PHA-activation of resting human lymphocytes measured by cryo-FISH. *Chromosome Res* 16(3):413–426.
13. Osborne CS, et al. (2004) Active genes dynamically colocalize to shared sites of ongoing transcription. *Nat Genet* 36(10):1065–1071.

14. Dundr M, et al. (2007) Actin-dependent intranuclear repositioning of an active gene locus in vivo. *J Cell Biol* 179(6):1095–1103.
15. Block GJ, Eskiw CH, Dellaire G, Bazett-Jones DP (2006) Transcriptional regulation is affected by subnuclear targeting of reporter plasmids to PML nuclear bodies. *Mol Cell Biol* 26(23):8814–8825.
16. Kukalev A, Nord Y, Palmberg C, Bergman T, Percipalle P (2005) Actin and hnRNP U cooperate for productive transcription by RNA polymerase II. *Nat Struct Mol Biol* 12(3):238–244.
17. Hofmann WA, et al. (2004) Actin is part of pre-initiation complexes and is necessary for transcription by RNA polymerase II. *Nat Cell Biol* 6(11):1094–1101.
18. Adelman K, Lis JT (2012) Promoter-proximal pausing of RNA polymerase II: Emerging roles in metazoans. *Nat Rev Genet* 13(10):720–731.
19. Core LJ, et al. (2012) Defining the status of RNA polymerase at promoters. *Cell Reports* 2(4):1025–1035.
20. Kim TH, et al. (2005) A high-resolution map of active promoters in the human genome. *Nature* 436(7052):876–880.
21. Guenther MG, Levine SS, Boyer LA, Jaenisch R, Young RA (2007) A chromatin landmark and transcription initiation at most promoters in human cells. *Cell* 130(1):77–88.
22. Hargreaves DC, Horng T, Medzhitov R (2009) Control of inducible gene expression by signal-dependent transcriptional elongation. *Cell* 138(1):129–145.
23. Escoubet-Lozach L, et al. (2011) Mechanisms establishing TLR4-responsive activation states of inflammatory response genes. *PLoS Genet* 7(12):e1002401.
24. Marshall NF, Price DH (1995) Purification of P-TEFb, a transcription factor required for the transition into productive elongation. *J Biol Chem* 270(21):12335–12338.
25. McKinstry KK, et al. (2007) Rapid default transition of CD4 T cell effectors to functional memory cells. *J Exp Med* 204(9):2199–2211.
26. Wells AL, et al. (1999) Myosin VI is an actin-based motor that moves backwards. *Nature* 401(6752):505–508.
27. Vreugde S, et al. (2006) Nuclear myosin VI enhances RNA polymerase II-dependent transcription. *Mol Cell* 23(5):749–755.
28. Heissler SM, et al. (2012) Kinetic properties and small-molecule inhibition of human myosin-6. *FEBS Lett* 586(19):3208–3214.
29. Avraham KB, et al. (1995) The mouse Snell's waltzer deafness gene encodes an unconventional myosin required for structural integrity of inner ear hair cells. *Nat Genet* 11(4):369–375.
30. Pavri R, et al. (2010) Activation-induced cytidine deaminase targets DNA at sites of RNA polymerase II stalling by interaction with Spt5. *Cell* 143(1):122–133.
31. Min IM, et al. (2011) Regulating RNA polymerase pausing and transcription elongation in embryonic stem cells. *Genes Dev* 25(7):742–754.
32. Danko CG, et al. (2013) Signaling pathways differentially affect RNA polymerase II initiation, pausing, and elongation rate in cells. *Mol Cell* 50(2):212–222.
33. Core LJ, Lis JT (2008) Transcription regulation through promoter-proximal pausing of RNA polymerase II. *Science* 319(5871):1791–1792.
34. Kim YJ, et al. (2013) HDAC inhibitors induce transcriptional repression of high copy number genes in breast cancer through elongation blockade. *Oncogene* 32(23): 2828–2835.
35. Rahl PB, et al. (2010) c-Myc regulates transcriptional pause release. *Cell* 141(3): 432–445.
36. Ferrai C, et al. (2010) Poised transcription factories prime silent uPA gene prior to activation. *PLoS Biol* 8(1):e1000270.
37. Dahmus ME (1996) Reversible phosphorylation of the C-terminal domain of RNA polymerase II. *J Biol Chem* 271(32):19009–19012.
38. Kaplan CD, Morris JR, Wu C, Winston F (2000) Spt5 and spt6 are associated with active transcription and have characteristics of general elongation factors in D. melanogaster. *Genes Dev* 14(20):2623–2634.
39. Brown KE, Baxter J, Graf D, Merkenschlager M, Fisher AG (1999) Dynamic repositioning of genes in the nucleus of lymphocytes preparing for cell division. *Mol Cell* 3(2):207–217.
40. Shen X, Ranallo R, Choi E, Wu C (2003) Involvement of actin-related proteins in ATP-dependent chromatin remodeling. *Mol Cell* 12(1):147–155.
41. Pestic-Dragovich L, et al. (2000) A myosin I isoform in the nucleus. *Science* 290(5490): 337–341.
42. Wada T, et al. (1998) DSIF, a novel transcription elongation factor that regulates RNA polymerase II processivity, is composed of human Spt4 and Spt5 homologs. *Genes Dev* 12(3):343–356.
43. Ardehali MB, et al. (2009) Spt6 enhances the elongation rate of RNA polymerase II in vivo. *EMBO J* 28(8):1067–1077.
44. Byun JS, et al. (2012) ELL facilitates RNA polymerase II pause site entry and release. *Nat Commun* 3:633.
45. Bieberstein NI, Carrillo Oesterreich F, Straube K, Neugebauer KM (2012) First exon length controls active chromatin signatures and transcription. *Cell Reports* 2(1):62–68.
46. Hendrix DA, Hong JW, Zeitlinger J, Rokhsar DS, Levine MS (2008) Promoter elements associated with RNA Pol II stalling in the Drosophila embryo. *Proc Natl Acad Sci USA* 105(22):7762–7767.
47. Henriques T, et al. (2013) Stable pausing by RNA polymerase II provides an opportunity to target and integrate regulatory signals. *Mol Cell* 52(4):517–528.
48. Ji X, et al. (2013) SR proteins collaborate with 7SK and promoter-associated nascent RNA to release paused polymerase. *Cell* 153(4):855–868.
49. Liu W, et al. (2013) Brd4 and JMJD6-associated anti-pause enhancers in regulation of transcriptional pause release. *Cell* 155(7):1581–1595.
50. Bond LM, Tumbarello DA, Kendrick-Jones J, Buss F (2013) Small-molecule inhibitors of myosin proteins. *Future Med Chem* 5(1):41–52.
51. Hacisuleyman E, et al. (2014) Topological organization of multichromosomal regions by the long intergenic noncoding RNA Firre. *Nat Struct Mol Biol* 21(2):198–206.
52. Kim LK, et al. (2007) Down-regulation of NF-kappaB target genes by the AP-1 and STAT complex during the innate immune response in Drosophila. *PLoS Biol* 5(9):e238.
53. Mortazavi A, Williams BA, McCue K, Schaeffer L, Wold B (2008) Mapping and quantifying mammalian transcriptomes by RNA-Seq. *Nat Methods* 5(7):621–628.

Supporting Information

Zorca et al. 10.1073/pnas.1502461112

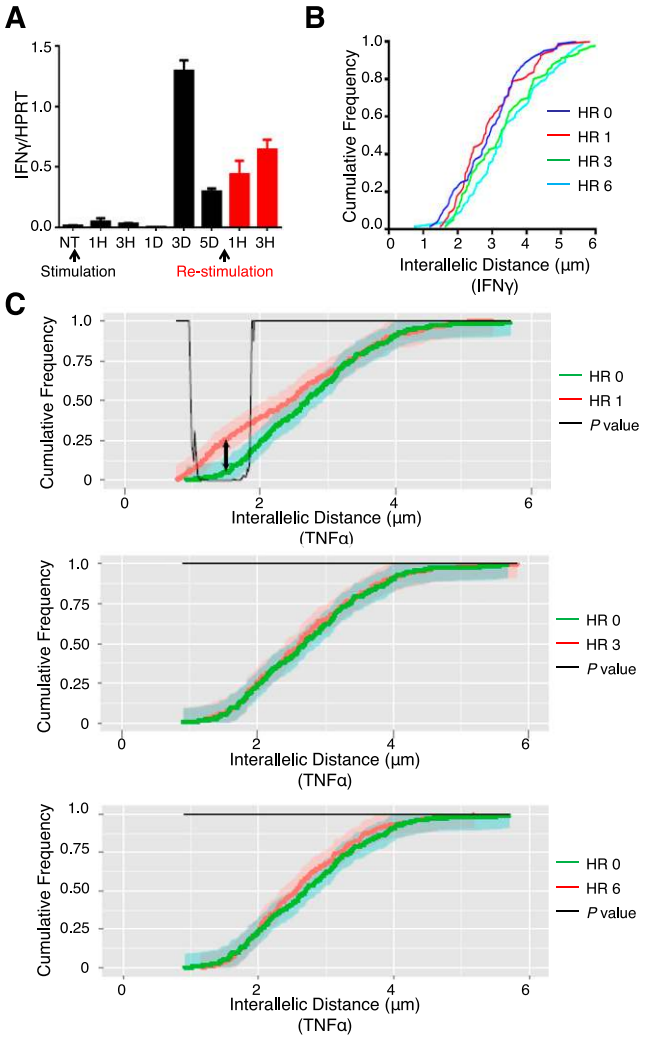

Fig. S1. Expression and nuclear localization of cytokine loci in T cells. (*A*) qPCR analysis of IFN-γ mRNA expression. Naive T cells from WT C57BL/6 mice were differentiated toward the Th1 lineage for 5 d and restimulated with plate-bound anti-CD3, and RNA was harvested at the indicated time points. HPRT, hypoxanthine phosphoribosyltransferase. (*B*) Three-dimensional DNA FISH for the *IFN-γ* locus in resting (HR 0) and restimulated (HR 1–6) Th1 cells. The cumulative frequency plots display interallelic distances for the *IFN-γ* locus over a time course of 1–6 h of anti-CD3 treatment ($n = 80$ cells per time point, representative of two independent experiments). The Kolmogorov–Smirnov (KS) test was performed, and statistical significance was not obtained for HR 0 vs. HR 1. (*C*) Selection of the cutoff value for allelic associations based on Fisher's exact test. Cumulative frequency plots showing changes in *LT/TNF* interallelic distances at 1 h (*Upper*), 3 h (*Middle*), and 6 h (*Bottom*) after TCR activation, compared with the resting (0 h) control. The shaded area around each cumulative frequency curve corresponds to a 95% confidence band, computed using the Dvoretzky–Kiefer–Wolfowitz inequality. Leftward shifts in the curves indicate closer association. We searched for a distance threshold that distinguished activated from resting conditions. Each of the 480 points was considered as a candidate threshold, and a series of Fisher's exact tests were performed to compare the proportion of interallelic distances above/below each threshold in the activated and resting conditions. Multiple comparison-corrected *P* values (Bonferroni correction; $n = 480$) for each test are overlaid on the cumulative frequency plots in black. Interalleic distance thresholds of 1.08–1.80 μm showed a significant difference ($P < 0.05$) between the 0-h and 1-h condition. No significant differences were found in the 0-h vs. 3-h or 0-h vs. 6-h condition at any distance threshold ($P >> 0.05$). We therefore selected an interallelic distance threshold of 1.5 μm, indicated by the arrow (*Upper*), because it falls in the center of that range. HR, hour.

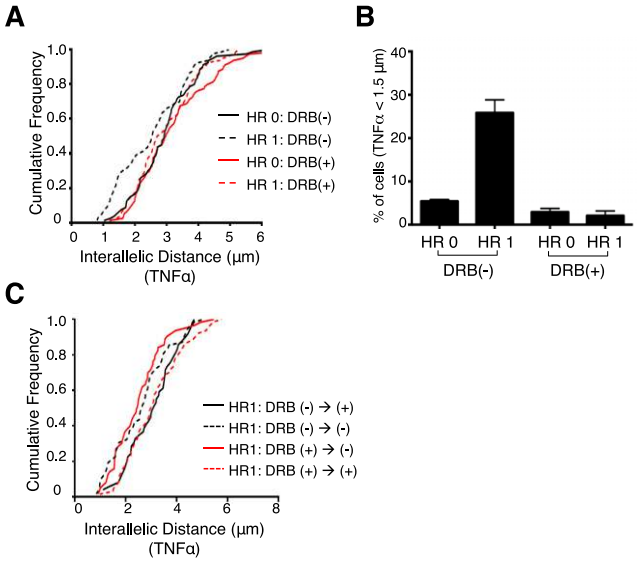

Fig. S2. Homologous pairing of the *LT/TNF* alleles is dependent on transcription. (*A*) Cumulative frequency plots display the separation of the homologous *LT/TNF* alleles in resting or 1-h restimulated Th1 cells in the presence or absence of DRB ($n = 80$ cells, representative of three independent experiments). The KS test was performed, and a P value <0.05 for HR 0 vs. HR 1 DRB (–) untreated Th1 cells was obtained. (*B*) Percentage of Th1 effector cells showing an interallelic *LT/TNF* distance equal to or below 1.5 μm. Data are averages of three independent experiments. The Student t test for HR 0 vs. HR 1 was performed. A P value <0.01 was obtained for DRB (–) untreated Th1 cells. Statistical significance was not obtained for DRB (+) treated cells. (*C*) DRB removal restored homologous *LT/TNF* allelic pairing. Th1 cells were treated with (+) or without (–) DRB before anti-CD3 restimulation either in the presence (+) or absence (–) of DRB. The cumulative frequency plots display *LT/TNF* interallelic distances. The KS test was performed, and a P value <0.01 for HR 0 vs. HR 1 for the DMSO control was obtained.

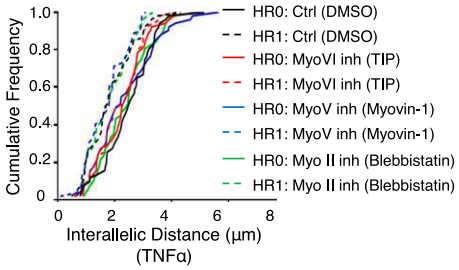

Fig. S3. Homologous pairing of the *LT/TNF* alleles is dependent on myosin VI (Myo VI) but not on Myo II or Myo V. The separation of the homologous *LT/TNF* alleles was measured in resting or 1-h restimulated Th1 cells in the presence or absence of the myosin inhibitors TIP, myovin-1, or blebbistatin ($n = 100$ cells). The KS test was performed, and a P value <0.01 for HR 0 vs. HR 1 for the DMSO control was obtained.

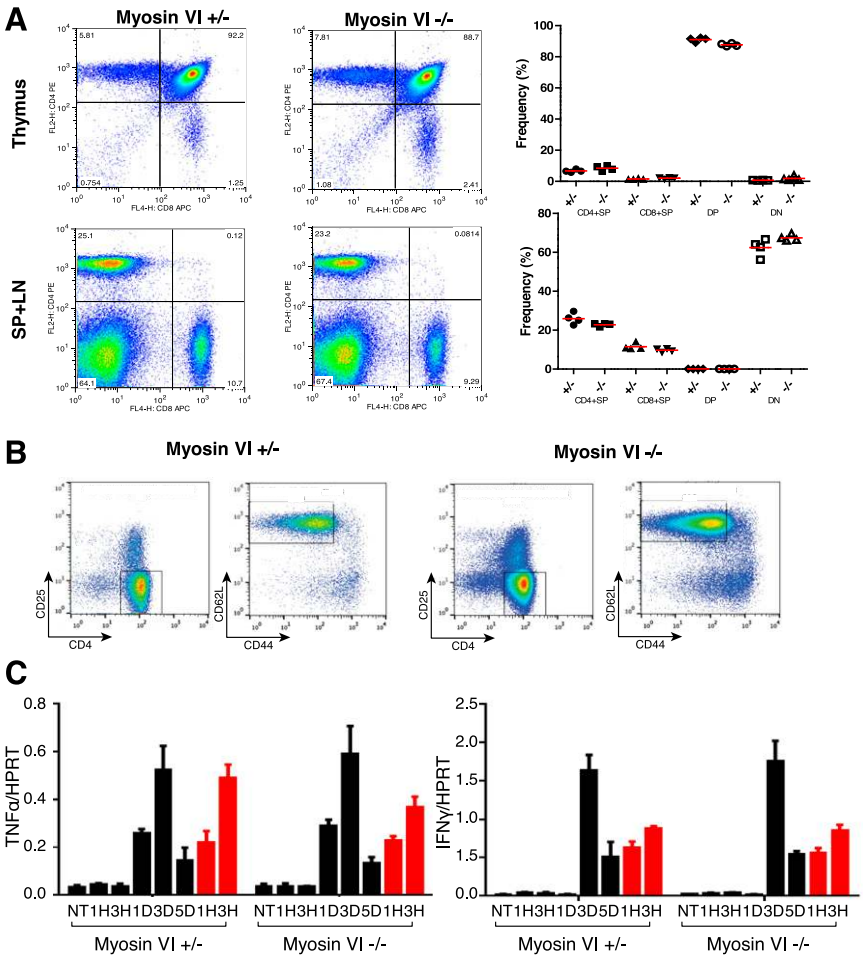

Fig. S4. Phenotypic characterization of myosin VI-sufficient and myosin VI-deficient T cells. (*A*) Nuclear myosin VI-deficient mice have normal frequencies of $CD4^+$ and $CD8^+$ T cells. Representative flow-activated cell sorting (FACS) plots display frequencies of $CD4^+$ and $CD8^+$ T-cell populations in the thymus and in the secondary lymphoid organs of myosin VI-sufficient and myosin VI-deficient mice ($n = 4$ mice, representative of three independent experiments). APC, allophycocyanin; DN, double negative; DP, double positive; PE, phycoerythrin; SP, single positive. (*B*) Representative FACS plots display frequencies of naive $CD4^+$ T-cell, effector memory, and central memory populations in secondary lymphoid organs of myosin VI-sufficient and myosin VI-deficient mice. (*C*) qPCR analysis of mature TNF-α and IFN-γ mRNA expression in myosin VI-sufficient and myosin VI-deficient cells over a time course of differentiation and activation.

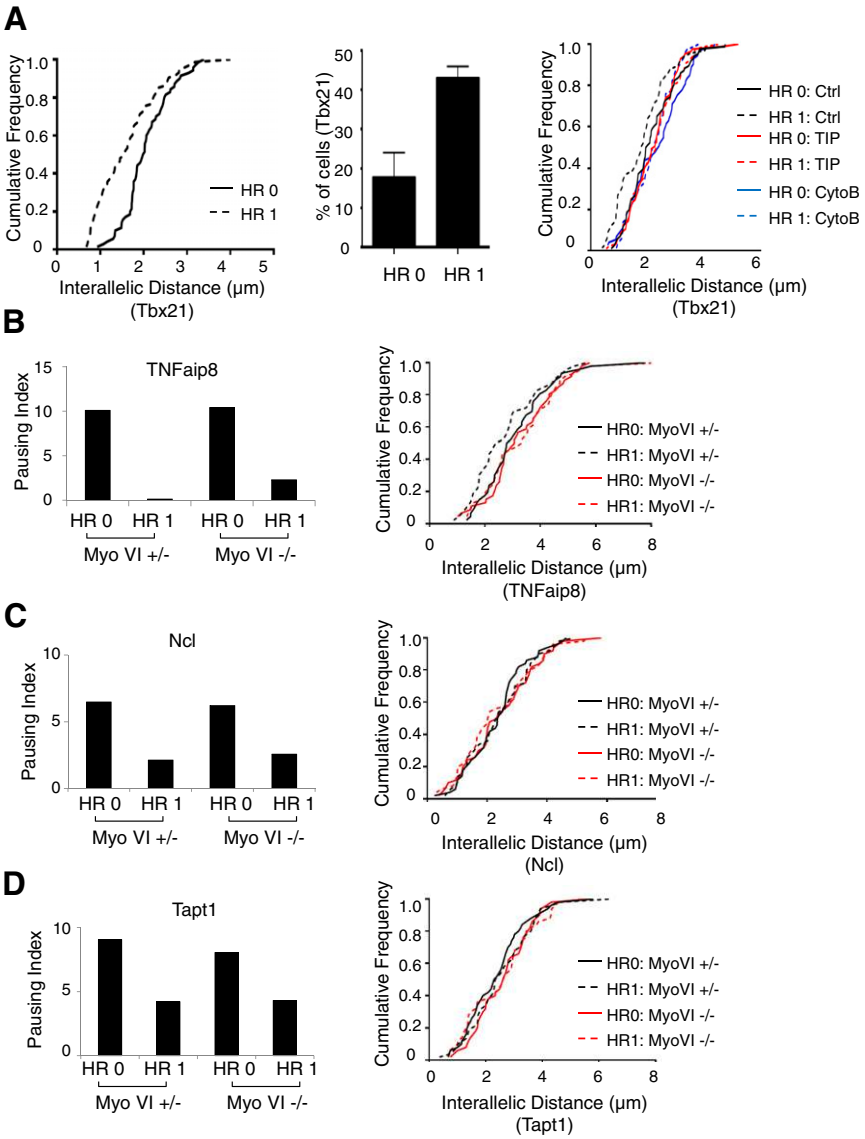

Fig. S5. Analysis of homologous pairing of myosin VI-dependent and independent genes. Four genes with similar PI values as *TNF* in resting (HR 0), Myo VI$^{+/-}$, and Myo VI$^{-/-}$ Th1 cells were analyzed by FISH for the ability to pair in response to TCR activation with anti-CD3 for 1 h (HR 1). The genes examined were *TBX21* with a PI of 7 (*A*; Fig. 3*B*), *TNFAIP8* with a PI of 10 (*B*), *NCL* with a PI of 6 (*C*), and *TAPT1* with a PI of 10 (*D*). For *A*, the myosin VI dependence of *TBX21* allelic pairing was examined by treatment with TIP or CytoB. Ctrl, control. For *B*–*D*, the PI value of the gene (*Left*) and the cumulative frequency plot of interallelic distances in resting (HR 0) and restimulated (HR 1) myosin VI-sufficient and myosin VI-deficient cells (*Right*) are shown (n = 100 cells per experiment).

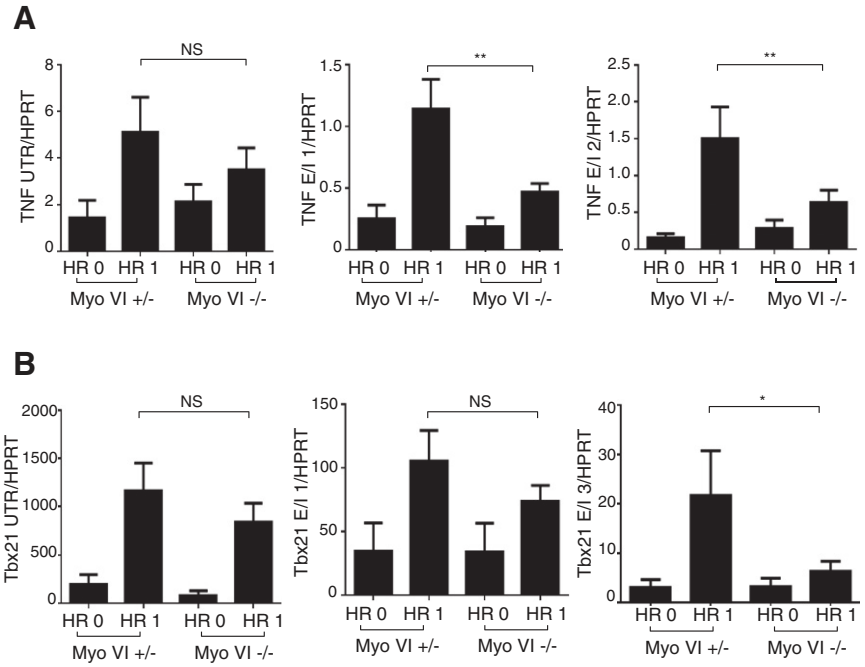

Fig. S6. Loss of myosin VI leads to decreased nascent TNF-α and Tbx21 mRNA expression upon TCR activation of Th1 cells. A qPCR analysis of nascent TNF-α (*A*) and Tbx21 (*B*) mRNA expression in resting or restimulated Myo VI$^{+/-}$ and Myo VI$^{-/-}$ Th1 cells was performed. The primers for qPCR were located within the 5′ UTR (*TNF* UTR), at the first exon/intron boundary (*TNF* E/I 1) or further along the gene body (*TNF* E/I 2 or 3). The results were averaged for three independent experiments. The Student *t* test was performed (*$P < 0.05$; **$P < 0.01$). NS, not significant.

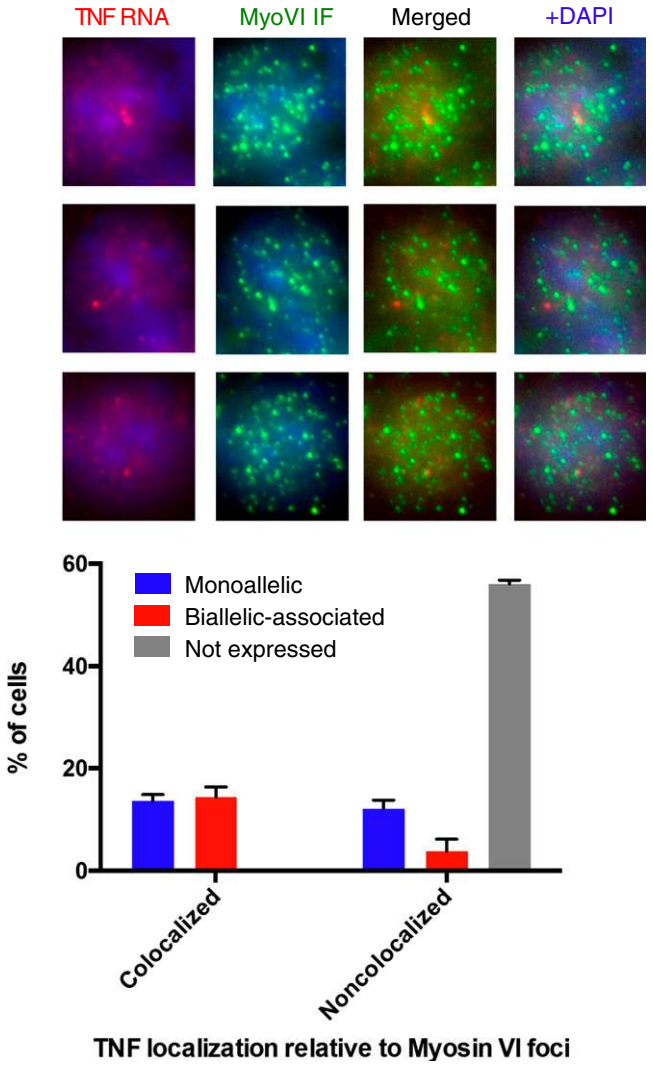

Fig. S7. Biallelically expressed *TNF* alleles colocalize with nuclear myosin VI foci. Immunofluorescence staining for myosin VI (green) was combined with single-molecule RNA FISH for TNF-α (red) to examine the localization of the active alleles in 1-h restimulated Th1 cells; two independent experiments; $n = 60$ cells. Nuclei were counterstained with DAPI (blue).

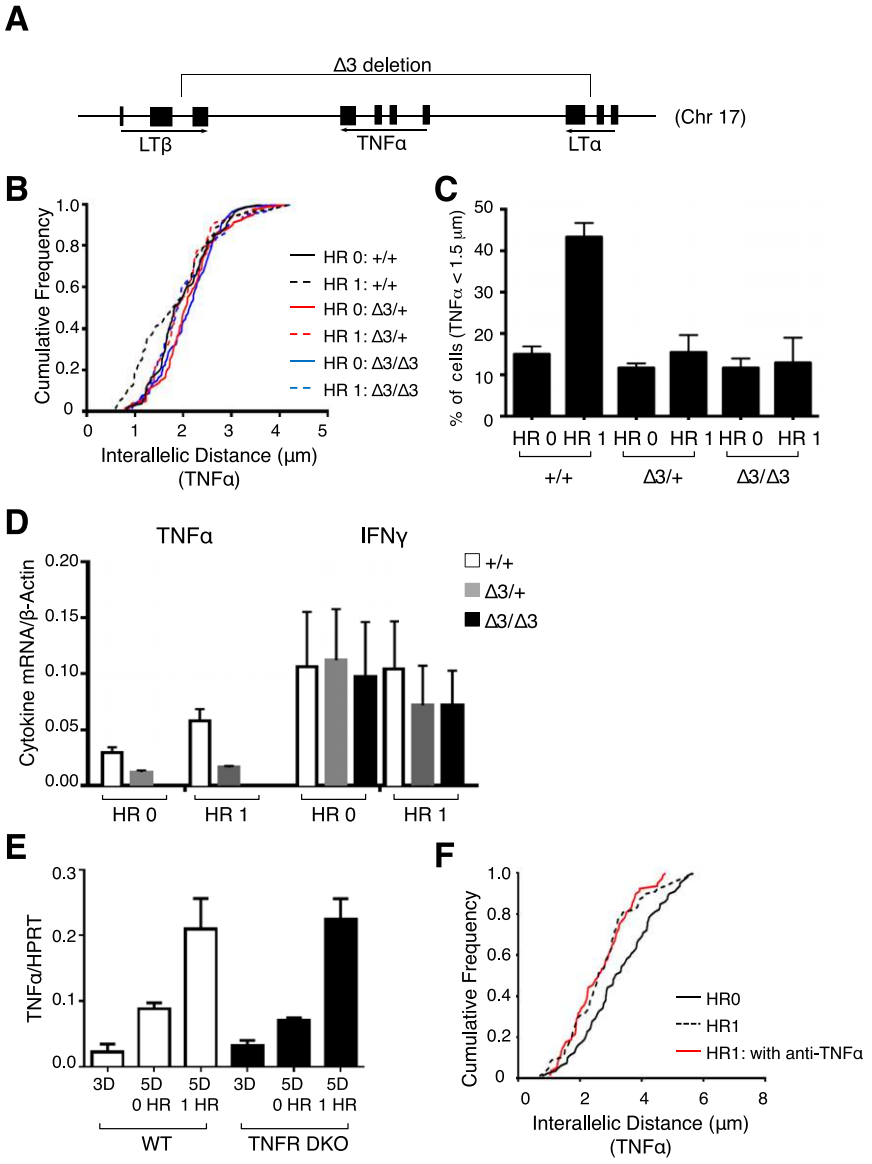

Fig. S8. Loss of homologous pairing perturbs TNF-α mRNA expression. (*A*) Genomic organization of the *LT/TNF* locus. The Δ3 deletion encompasses the entire *TNF* gene. (*B*) Cumulative frequency plots display the separation of the homologous *LT/TNF* alleles in resting or 1-h $^{+/+}$, TNF Δ3/$^{+}$, and Δ3/Δ3 restimulated Th1 cells (n = 80 cells, representative of three independent experiments). The KS test was performed, and a P value <0.05 for HR 0 vs. HR 1 for $^{+/+}$ Th1 cells was obtained. (*C*) Percentage of Th1 effector cells showing an interallelic *LT/TNF* distance equal to or less than 1.5 μm. Data are averaged for three independent experiments. The Student t test for HR 0 vs. HR 1 was performed. A P value <0.01 was obtained for $^{+/+}$ Th1 cells. No statistical significance was obtained for the Δ3/$^{+}$ or Δ3/Δ3 HR 0 vs. HR 1 comparisons. (*D*) qPCR analysis of mature TNF-α and IFN-γ mRNA expression in resting or restimulated $^{+/+}$, Δ3/$^{+}$, and Δ3/Δ3 Th1 cells. The results were averaged for three independent experiments. (*E*) qPCR analysis of TNF-α mRNA expression in differentiating (3D), resting (HR 0) or re-stimulated (HR 1) WT and TNFR double-KO (DKO) Th1 cells. The results were averaged for three independent experiments. (*F*) Cumulative frequency plots display the separation of the homologous *LT/TNF* alleles in resting or 1-h restimulated Th1 cells in the presence or absence of anti–TNF-α.